Mon. Not. R. Astron. Soc. **000**, 000–000 (0000) Printed 25 April 2001 (MN LaTeX style file v1.4)

A *ROSAT* medium sensitivity galactic plane survey $180^\circ < l < 280^\circ$

J.E. Morley[1], K.R. Briggs[1], J.P. Pye[1], F. Favata[2], G. Micela[3], S. Sciortino[3]

[1] *X-Ray Astronomy Group, Department of Physics and Astronomy, University of Leicester, Leicester LE1 7RH, UK*
[2] *Astrophysics Division - Space Science Department of ESA, ESTEC, Postbus 299, 2200 AG Noordwijk, The Netherlands*
[3] *Osservatorio Astronomico di Palermo, Piazza del Parlamento 1, 90134 Palermo, Italy*

Corrections 2001 April 25th

ABSTRACT

We have performed a moderately deep soft X-ray (0.1–2 keV) survey of the Galactic Plane using pointed observations with the *ROSAT* Position Sensitive Proportional Counter (PSPC). The survey is more than an order of magnitude more sensitive than previous X-ray surveys near the galactic plane. The data consist of 9 fields each of ≈ 10 ks exposure, pointed at positions on or very close to the galactic plane ($|b| < 0.3^\circ$) in the longitude range $180^\circ \lesssim l \lesssim 280^\circ$. This region has relatively low X-ray absorbing material out to distances of several hundred parsecs and presents fewer source-confusion problems than at other longitudes. The total sky area surveyed was 2.5 deg^2; this yielded 93 sources, 89 of which were detected in the 'hard' (0.4–2.0 keV) band. Nine sources were detected in both 'soft' (0.1–0.4 keV) and hard bands. In the hard band, the survey coverage is $\gtrsim 90$ per cent for sources brighter than 0.002 count s^{-1} ($\sim 2\times10^{-14}$ erg cm^{-2} s^{-1}), but falls steeply below this value, with the weakest sources being ~ 0.001 count s^{-1}. The median limiting flux is ≈ 0.0013 count s^{-1} ($\sim 1.3\times10^{-14}$ erg cm^{-2} s^{-1}). There are 64 sources with hard-band count rates > 0.002 count s^{-1}. We present the catalogue of X-ray sources and the number–flux relations ($\log N - \log S$). 18 sources have possible identifications from the SIMBAD database. We have searched the Tycho2 and USNO-A2.0 catalogues to find all possible optical counterparts brighter than $\sim$ 19th magnitude, and attempt to classify these on the basis of $\log(f_{\rm X}/f_{\rm opt})$vs. optical colour diagrams and near-infrared photometry from the 2MASS Second Incremental Data Release. Hence, we have found the majority of these sources to be consistent with being late-type main-sequence stars, as previous studies have proposed from incompletely-identified surveys. Comparison of the measured number–flux relations with predictions of galactic (stellar) and extragalactic populations support the view that the population of young stars in the plane is denser than previously thought.

Key words: catalogues – surveys – stars: late-type – galaxy: stellar content – X-rays: general

1 INTRODUCTION

Flux-limited surveys are important both in the study of source populations and in the identification of individual interesting objects. Using pointed observations from the *ROSAT* Position Sensitive Proportional Counter (PSPC), we present an X-ray source survey of the galactic plane reaching a factor ~ 5 lower in flux than previous 'galactic plane' surveys, namely the *Einstein* Galactic Plane Survey (EGPS; Hertz & Grindlay 1984, 1988) and the *ROSAT* Galactic Plane Survey (RGPS; Motch et al. 1991). The EGPS was a serendipitous source survey of Imaging Proportional Counter (IPC) fields at galactic latitudes $|b| < 15^\circ$, covering a total area of 275 deg^2, and detecting 71 X-ray sources above a flux threshold of $\sim 2 \times 10^{-13}$ erg cm^{-2} s^{-1} in the energy band 0.15–4.5 keV. The median and 90 per cent coverage fluxes were $\approx 7 \times 10^{-13}$ and $\approx 2 \times 10^{-12}$erg cm^{-2} s^{-1} respectively. The RGPS utilises the *ROSAT* PSPC All-Sky Survey (RASS) data for $|b| < 20^\circ$, with a typical limiting flux of a few times 10^{-13} erg cm^{-2} s^{-1}. Motch et al. (1991) have presented preliminary findings based on 225 sources detected in an area of ≈ 200 deg^2 in the longitude range $108^\circ < l < 155^\circ$. They have also presented analysis of a sample area covering 64.5 deg^2 centred on $l = 90°$, $b = 0°$ in which 128 sources were detected (Motch et al. 1997). The present survey, whilst covering a much smaller area of sky (≈ 2.5 deg^2, $180° \lesssim l \lesssim 280°$, $|b| < 0.3°$) than either the EGPS or RGPS, extends more than an order of magnitude deeper in flux, to $\sim 10^{-14}$ erg cm^{-2} s^{-1}, and has yielded 93 sources. Hence it complements well not only the EGPS and RGPS, but also *ROSAT* surveys at similar depths at high galactic latitudes (e.g. Hasinger et al. 1993; Branduardi-Raymont et al. 1994; Boyle et al. 1995).

The longitude range selected for our survey has relatively low X-ray absorbing material out to distances of several hundred parsecs and presents less confusion problems than at other longitudes. The restriction in latitude essentially removes scale-height effects when attempting to interpret the spatial distribution of sources, since $|b| = 0.3°$ corresponds to a height of only 5 pc off the plane at a distance from the Sun of 1 kpc. Previous surveys have typically found $\sim$ 80–90 per cent of identified sources to be active coronae, but left $\sim$ 40 per cent of detected sources unidentified (although Motch et al. (1997) were able to identify 98 per cent of sources at a threshold of 0.03 PSPC count s^{-1}: $\approx 3 \times 10^{-13}$ erg cm^{-2} s^{-1}). We try to classify the sources in our (deeper) survey on the basis of X-ray-to-optical flux ratios and optical and near-infrared colours, to find the percentage that are consistent with being due to active coronae.

The paper is organized as follows. In Section 2 we describe the data selection and the source-detection method. The determination of the number–flux relation is described in Section 3. Searches for optical counterparts are described in Section 4, and the methods used to classify these are detailed in Section 5. We compare our results to model predictions in Section 6, and summarise them in Section 7.

2 OBSERVATIONS

2.1 Data selection

The survey used 9 *ROSAT* (Trümper 1992) PSPC (Pfeffermann et al. 1986) fields, each of ≈ 10 ks exposure, to sample the galactic plane at longitudes from roughly 180° to 270° (the 'third quadrant')*. A log of the observations is given in Table 1, while Fig. 1 shows the distribution of the fields on the sky. Five of the pointings (numbers 1, 3, 4, 6 and 8) were specifically performed for this programme, while the remaining four datasets were obtained from the archive†.

The target objects for these latter pointings are noted in Table 1. The field positions were selected to avoid molecular clouds, strong ($\gtrsim 0.2$ PSPC count s^{-1}) known X-ray sources, bright stars and supernova remnants (SNRs), all of which might distort the survey. Each observation was required to have at least 8 ks exposure and to lie within 0.3° of the galactic plane. A reasonably uniform sampling in longitude was achieved for $180° \lesssim l \lesssim 250°$. The gap in the region $260° \lesssim l \lesssim 270°$ is due to the Vela supernova remnant. In order to provide some sampling in this area, we included in our analysis field number 9, at $l \approx 284°$. The most heavily sampled region is around $l \approx 230°$, with fields 5, 6 and 7.

2.2 Source detection

Our analysis was restricted to the inner 18 arcmin radius of each field. This utilised the portion of the PSPC field of view (FOV) with the highest sensitivity and spatial resolution, and avoided potential problems due to shadowing by the window-support structures. Those fields chosen from the archive also had the central 3.5 arcmin radius excluded from the analysis to prevent bias due to the central objects in these fields having been selected for their 'interesting' nature‡. Data intervals with poor aspect solutions (error $\gtrsim 1$ arcsec) or high anti-coincidence rates (Master Veto Rate > 170) were also rejected.

Images were made in three photon-energy bands: Total (0.1–2.0 keV, PI channels 11-202), Soft (0.1–0.4 keV, PI channels 11-42) and Hard (0.4–2.0 keV, PI channels 43–202). Each image had dimensions of 200×200 pixels^2, with each pixel being 15×15 arcsec^2. Sources were detected using the point-source search program PSS§. PSS required as input a data image and a corresponding background map.

The background map (one for each field and for each energy band) was constructed as follows. The average count rate was measured within the central 18-arcmin radius of an image. This was used for a preliminary PSS run. Detections made in this first run with a significance $> 4.0\sigma$ were then subtracted, and the resulting image smoothed using a $20{\times}20$ pixel^2 tophat function. This was used as the background model for a second (and final) PSS run where detections were accepted as X-ray sources if they exceeded a significance of 4.5σ.

A total of 93 sources was detected, however most of these (89) were also detected in the hard band and only 12 were detected in the soft band (3 of which were detected in the soft band only). Hence most of our work has concentrated on the hard-band results, with consideration of the soft-band data where appropriate. The hard-band detections and the hard-band upper limits on the three soft-only detections are shown in Table 2. Sources detected in the soft band are shown in Table 3. Also shown in Table 3 are the hardness ratios for each source, defined as $HR = (H - S)/(H + S)$, where H and S are hard- and soft-band count-rates respectively.

* Some workers, e.g. Paresce (1984), refer to this as 'Quadrant 4' or the 'Fourth Quadrant', while others, e.g. Frisch & York (1983) refer to it as 'Quadrant 3' or the 'Third Quadrant'. Here, we use the term '3rd Quadrant'.

† These were the *only* archive datasets that fulfilled our criteria when the data selection for the project was made, in 1994 August. This remains true.

‡ After completion of the analysis it was found that Field 9 did not have an on-axis target, and that the two target sources (compact open cluster Westerlund 2, and Wolf-Rayet star Wack 2134 , at off-axis angles of 7.8 and 8.0 arcmin) had been erroneously included in the survey. The effect of correcting for these two sources would be a small (< 1 per cent) reduction in survey area and the removal of two sources from the bright ($\gtrsim 0.03$ count s^{-1}) end of the number-flux relation. This would not change the results of the survey in any significant way.

§ PSS is part of the UK Starlink ASTERIX X-ray data analysis package (Allen 1992).

Table 1. Observation Log. The HI column density through the Galaxy in each field position is from Stark et al. (1992). The H_2 column density through the Galaxy in each field position was found by applying a conversion factor (X-ratio) of 2.0×10^{20} cm^{-2} to the CO maps of Dame et al. (1987). The total hydrogen column density was calculated as $N_{\rm H} = N_{\rm HI} + 2 \times N_{\rm H_2}$.

Field Nº	Obs-Seq	RA h m s	Dec ° ' "	l °	b °	$T_{\rm exp}$ (ks)	$N_{\rm HI}$	$N_{\rm H_2}$ 10^{20} cm^{-2}	$N_{\rm H}$	Notes
1	900627	5 45 37.6	28 56 10.0	180.00	0.00	9.52	51.5	15.0	81.5	GAL PLANE 1
2	200084	6 15 15.0	17 43 41.0	193.10	0.32	9.41	58.4	22.2	102.8	TARGET=G104-27
3	900426	6 42 25.8	04 23 17.0	208.00	0.00	10.42	62.7	09.0	80.7	GAL PLANE 2
4	900628	7 02 32.3	-05 23 54.0	219.00	0.00	8.59	67.7	11.2	90.1	GAL PLANE 6
5	900380	7 18 29.0	-13 13 03.0	227.75	-0.13	18.68	61.0	09.7	80.4	TARGET=NGC2359
6	900428	7 23 18.9	-15 08 33.0	230.00	0.00	9.84	69.2	09.7	88.6	GAL PLANE 3
7	200049	7 24 40.1	-16 12 03.6	231.09	-0.21	8.66	74.3	06.7	87.7	TARGET=HD58343
8	900427	8 10 02.8	-33 16 56.0	251.00	0.00	10.80	55.6	06.2	68.0	GAL PLANE 4
9	400329	10 24 58.5	-57 47 00.5	284.39	-0.28	9.00	–	39.7	>79.4	TARGET=1E102457

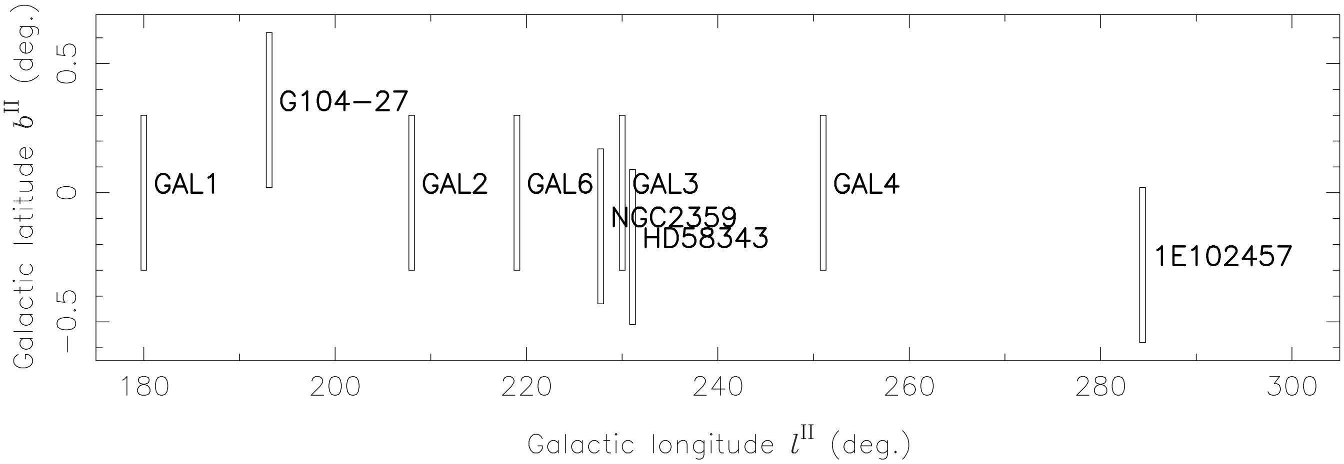

Figure 1. Relative positions of our fields along the plane. Each rectangle represents the longitudinal and latitudinal extent of the 18 arcmin radius field centre used in this survey.

3 THE NUMBER–FLUX RELATION

The detection count-rate threshold is a function of exposure time and of position in each PSPC field since it depends on background level and vignetting. The fields in our sample all have a *similar* distribution of thresholds, though they differ in detail. Thus each source will have its own associated coverage fraction within the survey, i.e. the fraction of the survey area within which it could be detected. Fig. 2(top) shows the hard-band coverage curve for the survey. Good coverage is achieved down to $\approx$ 0.002 count s^{-1}, with $\approx$ 90 per cent of the survey area being above this threshold. Below this count rate there is a sharp drop to $\approx$ 20 per cent coverage at $\approx$0.001 count s^{-1}. Fig. 2(bottom) shows the soft-band coverage curve.

Using the coverage curve it is straightforward to calculate the corrected number-flux ($\log N - \log S$) relation. For a source i, the fraction $f_{\rm i}$ of the survey area within which the source could have been detected was computed. That source then contributes $1/f_{\rm i}$ to the number-flux relation, which can be found by summing over the $1/f_{\rm i}$ values, as shown in Fig. 3.

3.1 Parametrization of the number-flux relation

The coverage-corrected, number-flux relation, for source count rate $S > 0.002$ count s^{-1}, was fitted with a power-law $N(>S) = N_0 S^{-\alpha}$, after first subtracting an 'extragalactic' component. The 'χ^2 ' fit was performed on the differential, binned form of the distribution, following the prescription of Lampton et al. (1976) to compute the confidence ranges.

The best-fit parameter values and 1-parameter 90% confidence intervals were α = 1.5 (1.1–2.2), and N_0 = 20 (13–25) sources per square degree above $S >$ 0.002 count s^{-1}. The joint normalisation–index confidence regions are shown in Fig. 4. The extragalactic contribution was estimated from published PSPC high-latitude source counts (Hasinger et al. 1993; Branduardi-Raymont et al. 1994 — both gave similar results) suitably attenuated by galactic absorption ($N_{\rm H} \sim 5 \times 10^{21}$ cm^{-2} , Stark et al. 1992), as explained in Section 3.2. The estimated extragalactic contribution to the total galactic-plane source counts is a relatively minor one; assuming zero contribution increases the normalisation to N_0 = 25 (18–32) and has little effect on the (already rather poorly constrained) power-law index.

Table 2. Sources detected in the hard band (0.4–2 keV) using the PSS source searching algorithm. Columns show source number, field in which source is detected, equatorial and galactic coordinates (J2000), significance of detection in equivalent Gaussian σ, count-rate and count-rate error in counts per ks, and notes. Of the 93 sources detected, 4 were not found in the hard band. Shown in this table is the upper limit on the countrate in the hard band for these sources. A letter S in the notes column indicates a source was detected in the soft band (0.1–0.4 keV) only whilst a T means the source was detected in the total band (0.1–2 keV) only.

RO	F	RA (J2000)	Dec	l (degrees)	b	Signif. σ	$C_X \pm \sigma_{C_X}$ (cts ks^{-1})		Notes
01	1	05 44 40.27	+28 57 35.3	179.871	-0.164	4.91	2.0	0.7	
02	1	05 44 41.22	+28 47 41.3	180.014	-0.247	5.06	2.8	0.9	
03	1	05 44 41.37	+29 07 37.2	179.731	-0.073	7.00	3.8	1.0	
04	1	05 44 45.69	+28 55 06.3	179.917	-0.169	6.11	2.3	0.7	
05	1	05 44 57.62	+28 58 40.4	179.889	-0.101	12.18	5.3	0.1	
06	1	05 45 07.19	+29 09 31.5	179.753	0.023	99%	< 0.8		S
07	1	05 45 13.11	+28 43 33.5	180.133	-0.184	7.83	4.5	0.1	
08	1	05 45 22.97	+29 10 59.5	179.762	0.084	13.56	8.9	0.1	
09	1	05 45 27.27	+28 57 46.7	179.958	-0.016	5.29	1.6	0.6	
10	1	05 45 56.84	+29 07 56.7	179.869	0.163	7.16	3.7	0.9	
11	2	06 14 23.50	+17 44 29.5	192.988	0.144	4.75	1.7	0.6	
12	2	06 14 35.95	+17 49 10.0	192.943	0.225	6.32	1.4	0.5	
13	2	06 14 41.85	+17 34 09.5	193.174	0.126	10.12	4.9	1.0	
14	2	06 14 42.27	+17 43 32.2	193.037	0.202	7.28	2.1	0.6	
15	2	06 14 46.78	+17 36 48.3	193.144	0.164	5.22	1.5	0.5	
16	2	06 15 17.57	+17 39 29.4	193.163	0.293	5.24	1.5	0.5	
17	2	06 15 34.03	+17 37 55.2	193.218	0.338	5.01	1.1	0.4	
18	2	06 15 43.23	+17 53 44.3	193.003	0.496	5.88	1.9	0.6	
19	2	06 15 47.51	+17 52 34.1	193.028	0.501	4.84	1.2	0.5	
20	2	06 15 54.51	+17 34 59.6	193.299	0.386	6.08	2.2	0.7	
21	2	06 16 05.30	+17 37 27.6	193.284	0.444	9.78	4.2	0.9	
22	2	06 16 24.75	+17 39 57.4	193.284	0.532	99%	< 1.4		S
23	3	06 41 29.91	+04 19 56.9	207.944	-0.231	5.03	3.6	1.0	T
24	3	06 41 36.16	+04 28 55.4	207.822	-0.139	11.60	6.8	1.1	
25	3	06 41 36.24	+04 31 41.9	207.781	-0.117	7.14	3.3	0.8	
26	3	06 41 50.69	+04 20 08.5	207.980	-0.152	13.52	5.6	0.9	
27	3	06 41 59.31	+04 28 47.9	207.868	-0.054	8.99	3.2	0.7	
28	3	06 42 13.47	+04 09 31.9	208.181	-0.149	4.68	1.8	0.6	
29	3	06 42 45.14	+04 23 21.8	208.036	0.073	8.36	2.7	0.7	
30	3	06 42 45.30	+04 18 40.2	208.106	0.038	10.22	3.6	0.8	
31	3	06 43 00.59	+04 25 16.7	208.037	0.145	5.01	1.3	0.5	
32	3	06 43 11.50	+04 12 42.1	208.244	0.089	7.58	3.5	0.8	
33	4	07 01 21.23	-05 26 42.4	218.906	-0.283	7.34	4.5	1.0	
34	4	07 01 22.42	-05 24 51.6	218.881	-0.264	11.29	7.0	1.2	
35	4	07 01 25.01	-05 22 22.0	218.849	-0.236	6.08	2.9	0.8	
36	4	07 01 52.48	-05 25 51.0	218.953	-0.161	33.55	23.2	2.0	
37	4	07 01 58.50	-05 36 18.7	219.119	-0.219	14.68	10.6	1.5	
38	4	07 02 05.87	-05 33 22.5	219.090	-0.169	6.14	2.1	0.7	
39	4	07 02 30.16	-05 10 40.5	218.799	0.093	6.10	2.5	0.8	
40	4	07 02 51.91	-05 14 16.5	218.894	0.145	13.61	6.7	1.1	
41	4	07 03 07.17	-05 35 19.7	219.235	0.041	12.55	8.2	1.3	
42	4	07 03 24.52	-05 27 29.2	219.152	0.165	5.29	2.5	0.8	
43	5	07 17 30.72	-13 05 23.1	227.527	-0.278	6.96	2.3	0.5	
44	5	07 17 32.64	-13 20 28.0	227.752	-0.388	7.46	2.6	0.5	
45	5	07 17 34.27	-13 17 47.2	227.716	-0.362	5.04	1.4	0.4	
46	5	07 17 41.39	-13 22 06.3	227.793	-0.370	5.56	1.8	0.5	
47	5	07 17 43.24	-13 25 23.3	227.846	-0.389	99%	< 0.5		S
48	5	07 17 49.17	-13 15 14.4	227.707	-0.288	8.91	1.8	0.4	
49	5	07 18 05.63	-12 58 28.3	227.491	-0.099	5.97	1.8	0.5	
50	5	07 18 06.08	-13 18 37.5	227.789	-0.254	6.48	1.3	0.4	
51	5	07 18 08.13	-13 19 58.1	227.812	-0.257	4.76	1.0	0.3	
52	5	07 18 10.83	-13 22 38.5	227.857	-0.268	8.37	1.9	0.4	
53	5	07 18 12.13	-13 06 34.4	227.623	-0.138	5.31	1.0	0.3	
54	5	07 18 13.02	-13 27 04.1	227.926	-0.295	6.42	2.2	0.5	
55	5	07 18 13.29	-13 23 54.8	227.880	-0.269	23.13	8.5	0.8	

Table 2. – *continued*

RO	F	RA (J2000)	Dec	l (degrees)	b	Signif. σ	$C_X \pm \sigma_{C_X}$ (cts ks^{-1})		Notes
56	5	07 18 38.49	-13 01 15.7	227.594	-0.002	6.98	2.1	0.5	
57	5	07 18 44.34	-13 06 47.5	227.687	-0.025	8.84	2.3	0.5	
58	5	07 18 48.47	-12 57 23.4	227.556	0.063	6.06	1.9	0.5	
59	5	07 19 10.30	-13 14 56.1	227.856	0.004	14.55	3.7	0.5	
60	6	07 22 25.08	-15 10 59.3	229.933	-0.210	5.61	2.5	0.8	
61	6	07 22 29.87	-15 04 04.6	229.841	-0.138	7.16	3.7	0.9	
62	6	07 23 05.23	-15 17 46.1	230.109	-0.121	9.07	2.7	0.7	
63	6	07 23 07.04	-14 58 41.3	229.832	0.035	5.31	1.7	0.6	
64	6	07 23 14.56	-14 52 51.2	229.761	0.107	6.05	2.7	0.8	
65	6	07 23 31.02	-15 12 20.6	230.078	0.012	9.20	3.4	0.8	
66	6	07 23 33.20	-15 10 29.9	230.055	0.035	4.73	1.2	0.5	
67	7	07 23 40.72	-16 08 09.3	230.916	-0.392	6.85	3.6	0.9	
68	7	07 24 01.68	-16 11 40.7	231.008	-0.346	5.19	1.4	0.5	
69	6	07 24 02.69	-15 05 24.8	230.037	0.179	7.54	2.6	0.7	
70	6	07 24 03.44	-14 57 16.1	229.919	0.246	4.70	2.0	0.7	
71	6	07 24 08.21	-14 59 29.6	229.960	0.245	5.31	2.3	0.7	
72	7	07 25 18.36	-16 10 35.1	231.137	-0.067	13.80	7.0	1.1	
73	7	07 25 21.41	-15 56 36.0	230.938	0.053	7.49	4.8	1.0	
74	8	08 09 24.01	-33 30 00.7	251.108	-0.232	5.92	5.4	1.7	
75	8	08 09 26.33	-33 20 15.2	250.976	-0.137	5.32	3.6	1.3	
76	8	08 09 26.95	-33 25 16.6	251.048	-0.180	6.34	4.7	1.5	
77	8	08 10 18.42	-33 06 10.3	250.879	0.143	4.99	2.4	1.0	
78	9	10 22 59.46	-57 42 41.6	284.128	-0.363	6.26	4.1	1.0	
79	9	10 23 38.83	-57 58 00.1	284.339	-0.532	5.33	3.1	0.9	
80	9	10 23 43.65	-57 38 33.8	284.175	-0.252	6.40	3.4	0.9	
81	9	10 23 50.65	-57 57 44.3	284.359	-0.514	5.44	2.8	0.8	
82	9	10 23 59.78	-57 45 34.8	284.268	-0.332	27.62	33.7	2.6	
83	9	10 24 14.97	-57 39 46.8	284.245	-0.232	5.43	1.9	0.6	
84	9	10 24 47.19	-57 32 54.8	284.245	-0.097	4.80	2.1	0.7	
85	9	10 25 01.52	-57 54 24.9	284.462	-0.384	4.92	2.0	0.7	
86	9	10 25 35.09	-57 50 50.8	284.493	-0.294	9.77	3.2	0.7	
87	9	10 25 45.58	-57 35 30.9	284.378	-0.065	10.28	6.7	1.2	
88	9	10 25 52.33	-57 54 00.0	284.554	0.318	5.97	2.3	0.7	
89	9	10 25 54.37	-57 37 57.4	284.416	-0.089	8.54	3.6	0.8	
90	9	10 25 55.13	-57 48 52.3	284.514	-0.243	68.29	95.5	3.9	
91	9	10 26 03.40	-57 59 15.5	284.621	-0.380	27.26	29.3	2.4	
92	9	10 26 04.09	-57 46 38.6	284.511	-0.201	5.34	2.2	0.7	
93	9	10 26 11.14	-57 56 55.8	284.615	-0.338	12.58	8.7	1.3	

Table 3. Sources detected in the soft band (0.1–0.4 keV) using the PSS source searching algorithm. Columns show the source number, field in which the source was found, coordinates, significance of detection, count-rate and count-rate error in counts per ks, and hardness ratio. Hardness ratio is defined as (H−S)/(H+S) where H is the hard band count-rate and S is the count-rate in the soft band.

RO	F	RA (J2000)	Dec	l (degrees)	b	Signif σ	$C_X \pm \sigma_{C_X}$ (cts ks^{-1})		HR $\pm \sigma_{HR}$	
06	1	05 45 07.19	+29 09 31.5	179.75318	0.02296	5.15	4.6	1.2	<-0.64	
16	2	06 15 17.57	+17 39 29.4	193.16395	0.29364	8.17	4.6	0.9	-0.51	0.14
21	2	06 16 05.30	+17 37 27.6	193.28400	0.44415	4.84	3.1	0.9	0.15	0.18
22	2	06 16 24.75	+17 39 57.4	193.28414	0.53188	6.26	5.5	1.2	<-0.69	
24	3	06 41 36.16	+04 28 55.4	207.82292	-0.13909	8.74	7.1	1.2	-0.02	0.12
25	3	06 41 36.24	+04 31 41.9	207.78194	-0.11763	4.99	4.0	1.1	-0.10	0.18
36	4	07 01 52.48	-05 25 51.0	218.95326	-0.16154	19.75	6.1	1.2	0.58	0.07
47	5	07 17 43.24	-13 25 23.3	227.84553	-0.38908	5.08	2.3	0.6	<-0.40	
67	7	07 23 40.72	-16 08 09.3	230.91691	-0.39249	7.62	5.8	1.2	-0.24	0.15
78	9	10 22 59.46	-57 42 41.6	284.12897	-0.36381	5.77	4.0	1.0	0.01	0.17
91	9	10 26 03.40	-57 59 15.5	284.62120	-0.38046	7.42	4.4	1.0	0.74	0.05
93	9	10 26 11.14	-57 56 55.8	284.61527	-0.33847	9.75	7.3	1.3	0.09	0.12

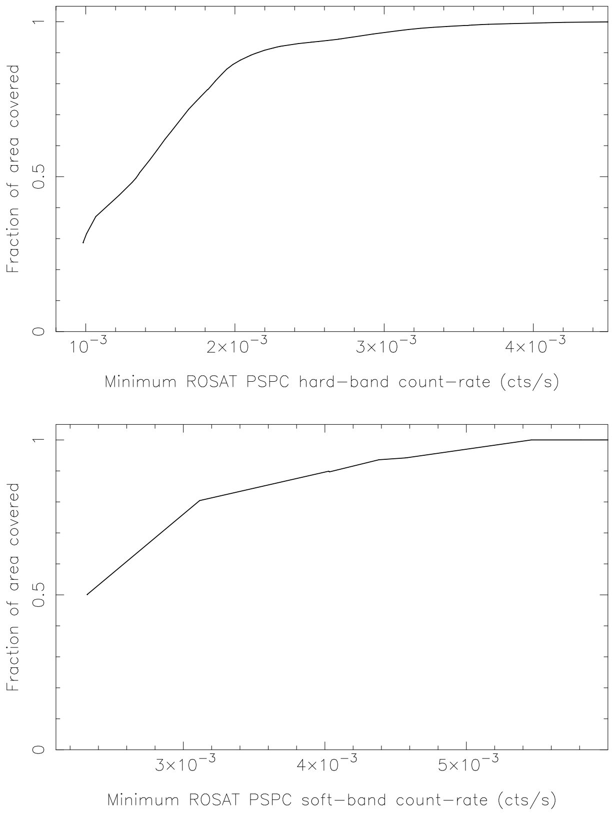

Figure 2. The coverage curves for the survey in the hard (top) and soft (bottom) bands. These take into account the differences in area between fields. Good coverage is achieved down to ≈ 0.002 ct/s in the hard band with around 90% of the survey being above this countrate.

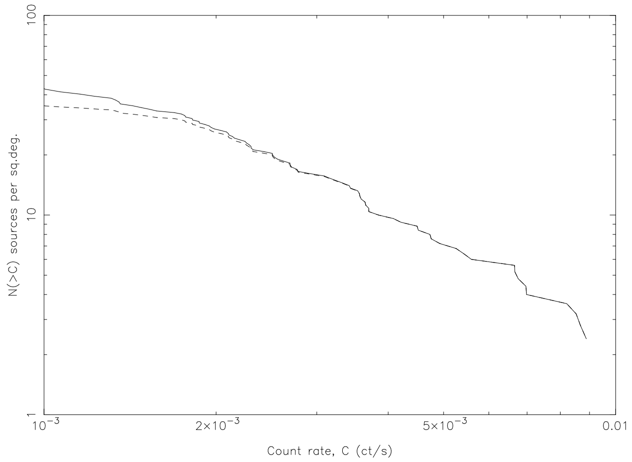

Figure 3. The hard-band (0.4–2.0 keV) number-flux relation, here shown in integral format, derived from the 89 hard-band sources detected in our 9 PSPC fields. The dotted line shows the raw-counts and the solid line shows the coverage-corrected $\log N - \log S$.

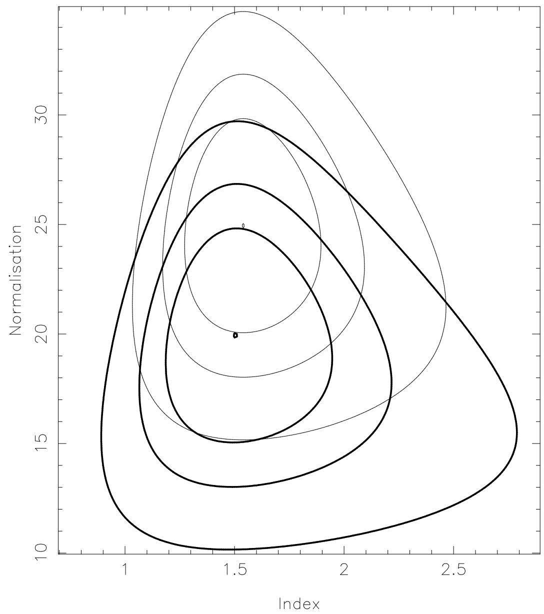

Figure 4. The 2-parameter, normalisation and index, power-law fit to the $\log N - \log S$. The extragalactic contribution has been subtracted, having been estimated using the high-latitude source counts from Hasinger et al. (1993) and allowing for transmission factors of 0.3 (lower, thicker contours) and zero (upper, thinner contours). Regions of 68, 90 and 99 per cent confidence are shown.

3.2 Contribution of extragalactic sources

The modification of the extragalactic number-flux relation by absorption in our own Galaxy was computed as follows. A 'galactic transmission factor' ($F_{\rm tg}$) was defined as $F_{\rm tg} = C_{\rm a}/C_{\rm u}$, where $\rm C_a$ is the count-rate from an extragalactic source after absorption by the interstellar medium (ISM) of our own galaxy, and $\rm C_{\it u}$ is the count-rate for zero galactic absorption. By considering a power-law spectrum with typical energy-index values (1–2) and $N_{\rm H} \approx 5 \times 10^{21}$ – 10^{22} cm^{-2}; cf. Table. 1) the hard-band $F_{\rm tg}$ was found to lie in the range ≈ 0.2–0.3. The nominal value was taken as 0.3; however the analysis was also conducted using 0.2 and 0.0, the latter corresponding to zero extragalactic source contribution. If the (unattenuated) extragalactic number-flux relation is $N_{\rm ex}(> S)$ sources per square degree at count rate S, then as viewed through the Galaxy, the number of extragalactic sources per square degree at count rate S' will be $N'_{\rm ex} = N_{\rm ex}(> S'/F_{\rm tg})$.

4 SEARCHING FOR OPTICAL COUNTERPARTS

We have searched for optical counterparts to our X-ray sources on the basis of positional coincidence and photometric properties alone (as in Briggs et al. 2000). We used four on-line all-sky databases in the following order. Firstly, SIMBAD was searched to find potential counterparts over a wide range of wavelengths. Secondly, we searched the Tycho-2 catalogue (Høg et al. 2000) for bright ($V \leq 12$) stellar counterparts. Thirdly, the USNO-A2.0 (Monet et al. 1998) catalogue was searched for all possible optical counterparts detected above the Palomar/ESO/SRC plate limit ($V \lesssim 19$). Finally, we searched the 2MASS Second Incremental Data Release (Cutri et al. 2000, go to www.ipac.caltech.edu) for near-infrared counterparts. The 2MASS photometry is more reliable than that found in the USNO-A2.0 and its three bands allow 2-colour diagrams to better constrain the class of the object. All potential counterparts are listed in Table. 4.

4.1 SIMBAD

We employed a uniform search radius of 35 arcsec around each X-ray source position. In our fields we would expect this search region to yield 4 SIMBAD objects by chance. We find SIMBAD counterparts to 29 of our sources. 11 matches are simply with X-ray sources detected in previous surveys, or in the field 9 observation already presented by Belloni & Mereghetti (BM94; 1994). No source was matched with more than one non-X-ray SIMBAD object. BM94 associated two sources with Wolf-Rayet stars and one with an O7 star. Source 11 was associated with a compact HII region¶ . Other stars accounted for 13 matches, in addition to two radio sources. All matches were found within 20 arcsec except for the brightest counterpart, a 6th mag. K-type giant 31 arcsec from source 81.

4.2 Tycho-2

Tycho-2 (Høg et al. 2000) is a catalogue of the 2.5 million brightest stars in the sky. It contains astrometric, proper motion and two-band photometric information based on data taken by the star-mapper on the ESA *Hipparcos* satellite. The catalogue's 90 per cent completeness level is at $V \sim 11.5$. The Tycho-2 search yielded all 13 stellar matches made in SIMBAD, and six further stellar candidates, with no ambiguous cases. Excepting the K-type giant, and a 12th mag star 32 arcsec from source 55, all matches were made within 20 arcsec of the X-ray source position. We converted the Tycho raw V_T and B_T band magnitudes to approximate Johnson photometry using the transformations: $V = V_T + 0.09(B_T - V_T)$ and $(B - V) = 0.85(B_T - V_T)$ (ESA 1997).

4.3 USNO-A2.0

USNO-A2.0 (Monet et al. 1998) is a catalogue of over 500 million objects, containing astrometric data and the blue and red magnitude for each, based on a re-reduction of the Precision Measuring Machine (PMM) scans of the POSS-I, SRC and ESO plates. The faintest objects in our region of interest are of 19th magnitude, and the catalogue is reportedly complete to $R \sim 18$, with the proviso that the source is detected on both blue and red plates. The PMM has problems in crowded fields, missing some obvious sources and detecting spurious sources. Excepting fields 5 and 9, the USNO seems unproblematic save for the odd obvious missed source and spurious detection (of order 1-10 per field). The centre of field 5 is dominated by the HII region NGC 2359, although none of our X-ray sources are in this area, while the west side of field 9 (closest to the Galactic Centre, and hence most densely populated) has considerable holes in its USNO coverage due to the HII region Gum 29 and the compact open clusters NGC 3247 and Westerlund 2, the latter housing one of our X-ray sources.

To keep the number of matches to a reasonable level we reduced our search radius to 20 arcsec. Previous experience with PSPC observations in the Hyades (Morley 1998) and the above SIMBAD and Tycho-2 searches indicate we would expect to miss $\lesssim 5$ per cent of counterparts. We found at least one USNO-A2.0 match for all but 7 of our 93 sources, although these 7 include source 81, with its bright counterpart 31 arcsec away, and source 82, which sits in a very confused region of stars in the heart of the open cluster Westerlund 2. We re-searched the catalogue using a search radius of 35 arcsec for these 5 unmatched objects and found matches for 3 of them, leaving only sources 19 and 73 without potential optical counterparts.

The number of matched objects per source varied from 0 to 7 and was field-dependent. The number of objects expected to fall into our search area by chance varied from < 1 in field 2 to > 4 in field 9, chiefly because the star-density increases along the plane from the anti-centre direction (fields 1 and 2), although if we consider only $R < 16$ this drops to < 1 even in field 9. In general, we expect multiple potential counterparts to each X-ray source.

4.4 2MASS

The Two Micron All Sky Survey (2MASS)(Cutri et al. 2000) is uniformly scanning the entire sky in three near-infrared bands (J (1.25 microns), H (1.65 microns), and K_s (2.17 microns)) for point sources brighter than about 1 mJy in each band. The Second Incremental Data Release covers $\sim$ 47 per cent of the sky, including 7 of our fields (fields 3 and 9 are not included), but has holes close to bright red stars (e.g. in field 2). This catalogue contains astrometric information and photometric magnitudes in the three bands, and a cross-correlation with objects in the USNO-A, making it ideal for following up the USNO search.

Using a 20 arcsec search radius, 185 matches were found, of which 42 were not coincident (within 5 arcsec) with USNO objects, including three faint potential counterparts to source 19, thus leaving source 73 as the only source with no potential optical counterpart.

5 CLASSIFICATION OF OPTICAL COUNTERPARTS

We have found more than one potential optical counterpart for most of our X-ray sources. We have treated each candidate as the real counterpart and classified it on the basis of its X-ray, optical and near-infrared photometry, and then made a judgement on the best classification for the source. Our classification procedure was as follows.

¶ IRAS 06114+1745. Classed an 'ultra-compact HII region' by Bronfman, Nyman & May (1996), detected as a water maser and considered a star-forming region by Palagi et al (1993), noted as 'nebulous' and associated with 'a B-type star that suffers appreciable circumstellar extinction' by Cohen, Jones & Walker (1989). Appears extended in optical and NIR images (and is proposed as a galaxy by Seeberger, Saurer & Weinberger (1996) on the basis of this extension), although it is not flagged as such in 2MASS; instead 12 point sources are detected in the region. These have peculiar, mostly heavily-reddened, near-IR colours and may be spurious or heavily absorbed stars within the cloud. Several HII regions are known to be associated with diffuse X-ray emission produced by hot plasma (e.g. Carina nebula, $L_X \sim 10^{35}$ erg s^{-1}).

5.1 X-ray to optical flux ratio

We have an optical magnitude (either V from Tycho-2, or R from USNO-A2.0) for the majority of our candidate counterparts and can compute upper limits ($R > 19$) for those found only in 2MASS, enabling us to calculate the X-ray to optical flux ratio for each candidate. This parameter is useful in attempts to identify and classify X-ray sources.

To convert X-ray count rate $C_{\rm X}$ (units: PSPC hard-band count s^{-1}) to flux $f_{\rm X}$ (units: erg cm^{-2} s^{-1}) in the nominal energy band 0.4–2 keV, we assume:

$$f_{\rm X} = 1.0 \times 10^{-11} C_{\rm X}$$

and for the optical (V-band) flux, $f_{\rm V}$ (units: erg cm^{-2} s^{-1} Å^{-1}):

$$\log f_{\rm V} = -0.4 m_{\rm V} - 8.43$$

(e.g. Allen 1973). Hence:

$$\log(f_{\rm X}/f_{\rm V}) = \log(C_{\rm X}) + 0.4 m_{\rm V} - 5.52$$

where $\log f_{\rm V}$ is now integrated over the 890 Å V-band width. The calculation for the POSS I E (red: $\lambda_0 \approx 6500$ Å) plate flux is very similar:

$$\log f_{\rm R} = -0.4 m_{\rm R} - 8.65$$

Hence:

$$\log(f_{\rm X}/f_{\rm R}) = \log(C_{\rm X}) + 0.4 m_{\rm R} - 5.05$$

where $\log f_{\rm R}$ is now integrated over the approximately 500 Å E-plate band width.

Extensive X-ray surveys (e.g. EMSS (Stocke et al. 1991); RGPS (Motch et al. 1998)) have found that, except at the high end of the flux distribution, the soft X-ray source populations are dominated by two classes: active coronae, and AGN. These surveys have also found these two classes of objects are readily separated on the basis of their X-ray to optical flux ratios. In general, AGN have $\log(f_{\rm X}/f_{\rm V}) > -1$ while active coronae have $\log(f_{\rm X}/f_{\rm V}) < -1$. Furthermore, active coronae show a saturation limit of X-ray luminosity at $\sim 10^{-3}$ of their bolometic luminosity so that earlier-type stars have more stringent limits upon their X-ray to optical flux ratio. This is well-demonstrated in the EMSS results (Stocke et al. 1991, Fig. 7) which plot $\log(f_{\rm X}/f_{\rm V})$ vs. $(B-V)$. We have formed approximate 90 and 98 per cent upper limits for coronal sources from this figure, which can be used to discriminate between coronal and non-coronal sources. Note that the EMSS boundary does not directly reflect the saturation limit of active coronae. If we calculate $\log(f_{\rm X}/f_{\rm V})$ for saturated main sequence (MS) stars from bolometric corrections (Schmidt-Kaler 1982) and plot this against $(B-V)$ (using MS colours of Johnson 1966) we find this 'saturation boundary' crosses the EMSS boundary at spectral type $\sim$ K0 and has a much shallower slope until the M-type stars when it steepens to a similar slope as the EMSS boundary, below which the saturation boundary remains by approximately one dex. This implies a fraction of the EMSS sample ($\sim$ 5–10 per cent) were detected while emitting above their nominal saturation limit, and we may expect some fraction of our sources to also be active coronae emitting above this limit, but to still be contained by the EMSS boundary (see Fig. 5).

5.1.1 *Tycho-2*

Given the flux limit of our survey and the magnitude limit of Tycho-2, we would expect all the counterparts found in this catalogue to be stars, and the majority of these to be active coronae. We have plotted these on a $\log(f_{\rm X}/f_{\rm V})$ vs. $(B-V)$ diagram to verify this and perhaps identify cases in which the Tycho-2 star is inconsistent with being an active corona (and hence is probably not the actual identification of the X-ray source).

Note that the EMSS and saturated boundaries assume zero absorption in the X-ray and optical and hence zero reddening, while we have plotted the observed reddened magnitudes and absorbed fluxes. Since the ratio of X-ray to optical flux is little-affected by absorbing columns with $N_{\rm H} \lesssim 10^{21}$cm^{-2}, and the optical absorption dominates over the X-ray attenuation for higher columns, we expect a plotted point to lie at higher $\log(f_{\rm X}/f_{\rm V})$ than its intrinsic position (Briggs et al. 2000). However, $B-V$ also increases with increasing absorption and the slope of the reddening vector in the diagram is shallower than the slope of the EMSS boundary so we do not expect any true coronal source to fall outside the 'coronal zone'. If we assume a reasonable absorption ($A_{\rm V} \leq 1.5$ mag/kpc), we estimate that the most luminous coronal source ($L_{\rm X} \approx 10^{31}$ erg s^{-1}) could not be detected in our survey through a column higher than $\sim 4 \times 10^{21}$ cm^{-2}, implying a shift in $\log(f_{\rm X}/f_{\rm V})$of no more than 0.5, and much smaller for less luminous sources. The mean error in the PSPC count rates is 25 per cent, which corresponds to $\pm$ 0.1 in $\log(f_{\rm X}/f_{\rm V})$, and the Tycho-2 photometric errors of $\leq \pm$ 0.1 mag. give errors of ± 0.04 in $\log(f_{\rm X}/f_{\rm V})$.

When we plot the 19 Tycho-2 sources on this diagram (Figure 5) only the counterparts to sources 55 and 75 fall outside the coronal zone. Both are within the errors, noted above, of the boundary, but we note that the candidate for source 55 is one of the two found more than 20 arcsec from its X-ray source.

5.1.2 *USNO-A2.0*

We encounter two problems in performing the same test using USNO photometry. Firstly, the blue and red magnitudes are photographic magnitudes that only roughly approximate to Johnson B and R band magnitudes. Fields 1–7 are covered by POSS-I O and E plates, while the southerly fields 8 and 9 are covered by the SRC J and ESO-R F plates, although the photometric solutions in the USNO-A2.0 catalogue do not account for bandpass differences between the two sets of red or blue plates. Therefore, we use the POSS-I bandpasses here. Humphreys et al. (1991) determined the colour transformations $O-B$ and $E-R$ as functions of $B-V$ and $V-R$ respectively. $O-B$ is a very weak function of $B-V$ and has the small range of 0–0.2 for mid- and late-type stars ($B-V > 0$), which is within the quoted USNO-A2.0 photometric errors, so we make the approximation $O \approx B$. E can be transformed using the relation:

$$E - R = -0.011 + 0.148(V-R) + 0.058(V-R)^4$$

for $-0.2 < V-R < 1.7$. The relation is flatter at redder colours.

We transformed the coronal boundary by using this relation and the mean intrinsic colours for main sequence stars

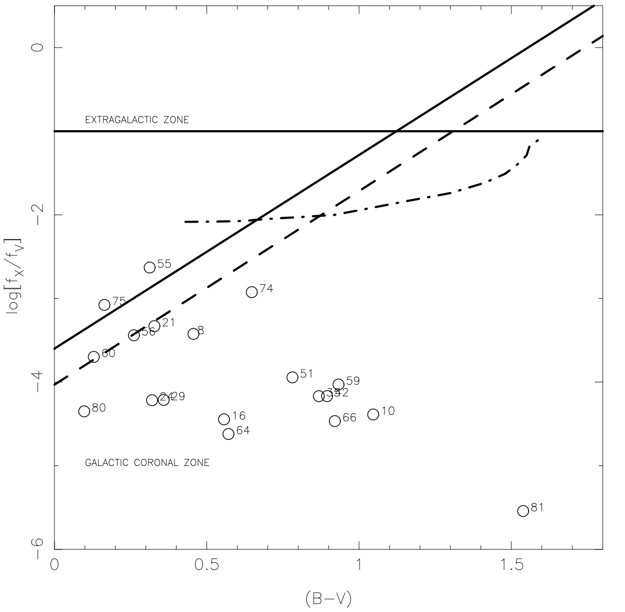

Figure 5. Plot of $\log(f_{\rm X}/f_{\rm V})$vs. $B-V$ for all potential optical counterparts found in the Tycho2 catalogue. The plotted quantities are not corrected for reddening or absorption. Numbers refer to the associated X-ray source. The bold diagonal solid and dashed lines are expected to bound zones of the diagram containing, respectively, 98 and 90 per cent of coronal sources (derived from fig. 7 in Stocke et al. 1991). The bold horizontal line marks the value above which extragalactic sources are expected to dominate. The bold dot-dashed line indicates the saturation threshold of $\log(L_{\rm X}/L_{\rm bol})= -3$ for main sequence stars.

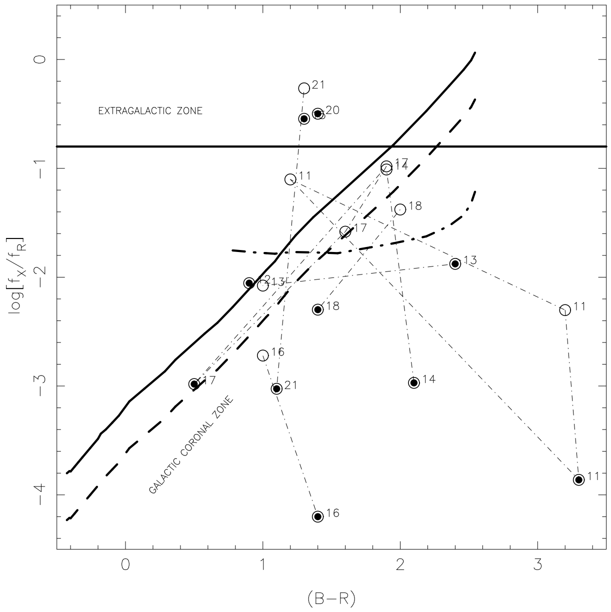

Figure 6. Plot of $\log(f_{\rm X}/f_{\rm R})$vs. $B-R$ for all potential optical counterparts to X-ray sources in field 2 found in the USNO-A2.0 catalogue. The plotted quantities are not corrected for reddening or absorption. The coronal and extragalactic boundaries and the saturation threshold are indicated using the same bold lines as in Fig. 5. Fine dot-dashed lines join candidate counterparts to the same X-ray source. A filled circle indicates the counterpart found deepest in the coronal zone, or the brightest counterpart where there is no coronal counterpart.

(i.e. $V-R$ vs. $B-V$) measured by Johnson (1965). We converted the extragalactic boundary by applying the measured mean $(V-R)$ for a sample of bright radio galaxies (Machalski & Wisniewski 1988) of +0.91 (±0.12), shifting the boundary to $\log(f_{\rm X}/f_{\rm R})$= -0.8. Secondly, the USNO photometry is not well-constrained. The reported accuracy is ± 0.2 mag. but there are a number of cases where we see discrepancies much greater than this. While this does not strongly affect the accuracy of $\log(f_{\rm X}/f_{\rm R})$, it can make the $B-R$ colour unreliable. This is a strong motivation for using the 2MASS catalogue for photometric information where available.

We plotted the counterparts on a $\log(f_{\rm X}/f_{\rm R})$ vs. $B-R$ diagram a field at a time and classified each according to the region ('Extragalactic' (E), 'Coronal' (C) or 'Neither' (or 'No Man's Land') (N)) in which it fell. We only show the diagram for field 2 here (Fig. 6), as the many potential counterparts in some fields make the diagrams very crowded. Many candidates fell in the 'Extragalactic' zone, which is not unexpected: while we expect most true AGN to be so heavily absorbed as to be undetectable in the optical ($V\sim 19-24$), many faint background stars that fall into the error circles by chance and are not associated with a detected X-ray source should fall in this region of the diagram. A surprisingly high number of bright counterparts fell into 'No Man's Land'. The only sources we expect to find in this region are the easily-absorbed white dwarfs and the comparatively sparse accreting binaries.

Accepting the BM94 identification of three sources with (non-coronal) early-type stars, 50 sources were found to have 'coronal' candidates, one of which SIMBAD reveals to be a compact HII region. Considering the brightest candidates to the remaining sources, 25 were classed 'No Man's Land', 12 'extragalactic' with 3 unidentified.

The larger-than-expected number of 'No Man's Land' objects may be due to (a) a fainter counterpart being the correct identification, (b) an unrecognised population of low $f_{\rm X}$ X-ray sources or (c) inaccurate (too blue) colours in the USNO-A2.0 catalogue. Fainter counterparts would mean higher $\log(f_{\rm X}/f_{\rm R})$and point to an unreasonably large number of extragalactic detections. We have used 2MASS near-IR colours to indicate whether candidates are consistent with being MS stars, and hence highlight unusual objects or inaccurate $B-R$ values.

5.2 Near-infrared 2-colour diagram

We plotted all 2MASS potential counterparts on a $J-H$ vs $H-K_{\rm S}$ diagram upon which we superimposed an empirical locus for MS stars (from Bessell & Brett 1988$\|$) and defined a box region (from consideration of the quoted photometric errors) within which objects could be considered consistent with being MS stars** (Fig. 7). The 2MASS data has given

$\|$ Fortuitously the 2MASS colours are well-matched to the Bessell & Brett colours

** The locus for giant stars does not diverge from the MS locus until K5 III which is beyond the coronal dividing line (Ayres et al. 1981, Haisch & Simon 1982), so we do not expect to exclude any X-ray emitting giant sources. This box region is consistent with some insight into whether objects that fell into the 'N' region of the $\log(f_X/f_R)$vs $B-R$diagram did so due to errors in the USNO colours, or because they are not coronal sources. Of the 14 sources whose brightest and/or reddest counterparts fell in 'No Man's Land' and were covered in the 2MASS Second Incremental Data Release, 7 have near-IR colours consistent with being MS stars and $\log(f_X/f_R)$values consistent with active coronae, strongly suggesting that the errors are in the USNO colours and most of the 'N' class sources are actually coronal (see Fig. 7).

For objects within photometric error of the MS locus and with $\sigma_{J-H} \leq 0.1$, we have estimated the spectral type by comparing primarily $J-H$and secondarily $H-K_S$colours (not accounting for any possible reddening – the reddening vector for $A_V = 2$ is shown in Fig. 7) to the MS NIR colour tables of Bessell & Brett (1988)[††]. The classification criteria are shown in Table 5. Candidate counterparts to source 11 (the HII region) have been excluded. The sample includes 83 potential counterparts to 47 X-ray sources. Fig. 8 shows the distribution of this sample by estimated spectral type. A crude attempt has also been made to weight each counterpart according to its likelihood of being the correct identification for the X-ray source. This judgment was made on the bases of optical brightness (probability that an object of that brightness would appear within 20 arcsec of an X-ray source position by chance alone) and $\log(f_X/f_{\rm opt})$vs. estimated spectral type. Each candidate was given a weighting from 0 to 1 in grades of 0.2 such that the sum of weightings for all candidates to any particular X-ray source was 1. The resultant distribution among spectral types is shown in Fig. 8 using a dashed line. There are no major differences between the total and weighted distributions. K-type stars are the most frequent counterparts. We estimate $\sim$ 12 sources are M-type stars, although the photometric selection criteria of the sample do bias against the least-luminous spectral type.

To further investigate the USNO colours, we took all the matches within 2 arcsec between 2MASS and USNO-A2.0 catalogues in a single field, estimated spectral types exactly as above, and compared the distribution of USNO colour for each spectral type with the expected range of these colours. F-stars peaked $\sim$ 0.2 mag lower than the expected minimum, but had a long tail extending to $B-R\sim 3$. G-stars peaked $\sim$ 0.5 mag lower than expected with a sharp low cutoff at 0.2 and a steady slope to $\sim$ 3.5. This means that the mean for F and G stars is actually *much higher* than expected, although the RMS scatter is 1 mag. The K-star distribution was more Gaussian with a peak and mean within the expected range with RMS spread of 1 mag. The M-star distribution was also more Gaussian-like, with a mean in the expected range and RMS scatter of 0.7 mag, and a fairly sharp lower cutoff around 1.3. The expected effect of reddening is for the true spectral type to be *earlier* than estimated yet for $B-R$to be still *higher* than appropriate for the estimated spectral type. Heavy reddening may explain the long tails on the F and G

the spread observed by Finlator et al. 2000, with an allowance for reddening equivalent to $A_V = 2$

†† Finlator et al. (2000) conclude that spectral types cannot be accurately estimated from 2MASS colours alone, although stars later than K5 are well-separated from those earlier than G5.

Table 5. Criteria for defining spectral type via 2MASS colours (adapted from the colour tables of Bessell & Brett (1988)). The effects of reddening are not included. Note that the class labelled 'km?' has $J-H$ lower than M-type stars but $H-K_S$ higher than K-type stars. This could be due to reddening or to scatter in $J-H$ or $H-K_S$. These objects have been tentatively classed with the M-type stars in Fig. 8.

Sp. Type	$J-H$	$H-K_S$
A	0.00–0.10	<0.15
F	0.10–0.30	<0.15
G	0.30–0.40	<0.15
K0-K2	0.40–0.50	<0.15
K2-K7	0.50–0.80	<0.15
km?	0.50–0.60	>0.15
M	0.60–0.80	>0.15
gM	>0.80	>0.15

distributions. While this indicates that objects certainly *may* have colours that are significantly too blue for their spectral type, it does not point toward a systematic trend.

We have estimated the X-ray luminosity of those sources with counterparts in the Tycho-2 catalogue that have published spectral types or spectral types estimated from well-constrained 2MASS colours ($\sigma_{J-H} \leq 0.1$). A distance modulus (not corrected for absorption) was calculated for each star using the absolute magnitudes of Schmidt-Kaler (1982), which was converted into a distance used to calculate the (0.4–2.0 keV) X-ray luminosity from the hard-band flux listed in Table 2. These estimated distances and luminosities are listed in the final column of Table 4. The neglect of absorption in this procedure may underestimate the true luminosity, but this should be a small problem in the hard band. The high luminosity of source 55 ($\log(L_X)\sim 31.0$ erg cm^{-2} s^{-1}) if 55C is the counterpart rules out this late-A type star as a candidate (recall it was also >30 arcsec from the source position).

The bulk of 2MASS galaxies in off-plane directions are found with $0.2 \leq (H-K_S) \leq 0.6$ and $0.6 \leq (J-H) \leq 0.9$ (Cutri et al. 2000). As the typical column through the Galaxy in each field of $N_H \sim 10^{22}$ cm^{-2} implies $A_V \sim 5$ mag. we would expect any galaxies among our counterparts to sit well above and to the right of the MS locus. None of our 'extragalactic' candidates actually occupies this part of the 2-colour diagram, which suggests that they are chance associations with stars rather than the true optical counterparts, which must be fainter and hence have higher $\log(f_X/f_R)$. Indeed, many of the 'extragalactic' candidates have 2MASS colours consistent with MS stars (see Table 4).

5.3 Hardness ratios

We calculated hardness ratios $(H-S)/(H+S)$ for all twelve sources detected in the soft band (see Table 3). Previous surveys have found such ratios useful in distinguishing between sources of different types (e.g. Motch et al. 1998, Haberl and Pietsch 1999, Haberl et al. 2000). Unabsorbed coronal sources typically have HR$\sim$0, but can have values significantly higher (if they are heavily absorbed, or flaring) or lower (if they have intrinsically cooler coronae). The hardest source is the flaring source 91. The softest source detected

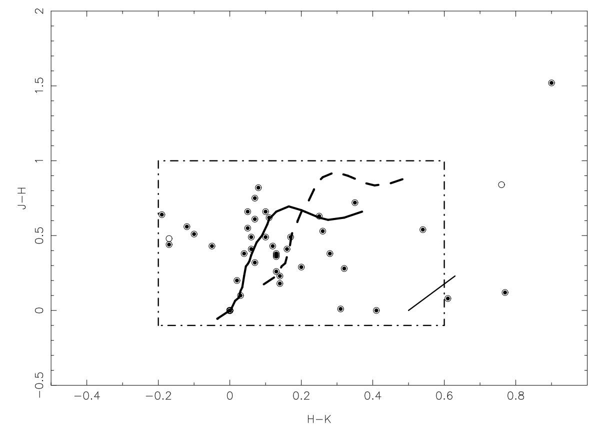

Figure 7. Near-infrared 2-colour diagram for N-type sources (as classified in Fig. 5 or Fig. 6), found in the 2MASS Second Incremental Data Release. Open circles indicate non-detections in the K_S band. The bold line shows the main sequence (MS) locus of Bessell and Brett (1988), while the bold dashed line shows the same locus reddened by absorption of $A_V = 2$. This reddening vector is also shown. We used the dot-dashed box to define objects that were consistent with being MS stars. Note that the majority of these objects are consistent with being MS stars.

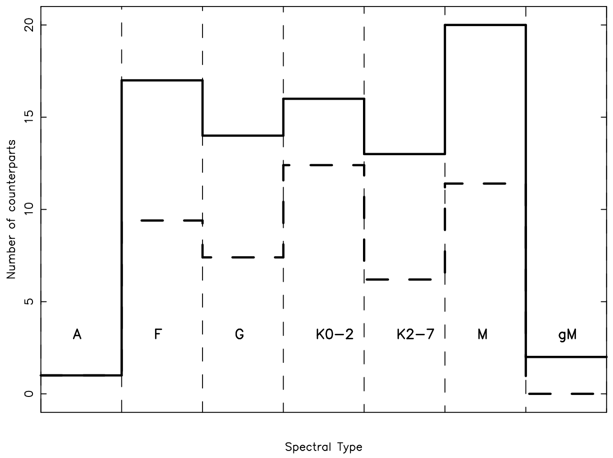

Figure 8. Histogram of spectral types estimated by comparison of 2MASS photometry to the MS NIR colour tables of Bessell & Brett (1988). The classification criteria are shown in Table 5. Only objects within photometric error of the MS locus and $\sigma_{J-H} \leq 0.1$ are included in the sample of 83 candidates to 47 X-ray sources. The solid line includes all 83 counterparts; the dashed line is weighted such that each X-ray source contributes 1 to the sample (see text for details).

in the hard band is source 16 whose most-likely counterpart is the 10th mag (possibly G-type) star GSC 01318-00940. Three sources were detected only in the soft band. Hot white dwarfs (WDs) are typically very soft sources, but their flux is easily absorbed so they cannot be seen to great distances in heavily-obscured regions like the galactic plane. None of our soft sources has a counterpart with the blue colours expected of a WD, although an X-ray emitting WD could be hidden by an optically brighter companion. Sources 6 and 47 may be such systems, although source 22 is not. We have estimated the only counterpart, 22A, to be a mid-M dwarf. While the X-ray source is much softer (HR≤ -0.69) than a typical active dM star, such as 67A (which is very similar photometrically (see Table 4) but has HR$= -0.24$), the dM star is too faint to hide a hot WD in the system.

5.4 Classifying sources

In the crowded region of the Galactic Plane, it is near-impossible to determine the correct counterpart to each X-ray source without good-quality spectra of the candidates, which would require an extensive optical observing program. However, we seek to test the hypothesis that the majority of X-ray sources in the galactic plane are due to coronal emission from late-type stars. Therefore, if there is any object in the X-ray source's error circle we may classify as 'coronal', we consider that source to be consistent with being coronal. Our classification procedure is as follows.

A candidate is classed *coronal* if: (a) it falls in the coronal zone of the Tycho-2 $\log(f_X/f_V)$vs $B-V$ or USNO-A2.0 $\log(f_X/f_R)$vs $B-R$ diagram *and* any available 2MASS photometry does not rule out a MS star; or (b) it falls in the 'No Man's Land' region of the $\log(f_X/f_R)$vs $B-R$ diagram and 2MASS photometry is consistent with that of a MS star. It is classed '*extragalactic*' if it falls in the extragalactic zone of the $\log(f_X/f_R)$vs $B-R$ diagram *or* appears in 2MASS only. Note that the most active late-type stars may be counted as extragalactic if their USNO colours are erroneously blue, but the 2MASS colours should discriminate between the galaxies and the latest-type stars and any candidates we misclassify in this way must be emitting above their nominal saturation threshold. It is possible that embedded objects, such as protostars, may also be erroneously included in this class. There are several objects around the HII region associated with source 11 that are seen only in 2MASS with very red colours; these are possibly embedded objects, but unlikely to contribute to the X-ray flux of source 11, as the HII region is too distant. '*No Man's Land*' candidates are those that fall into that region of the $\log(f_X/f_R)$vs $B-R$ diagram *and* have either no or non-MS 2MASS photometry. '*Other*' classifications (e.g. early-type stars, and HII regions) come from SIMBAD, while '*Unidentified*' sources are those for which we could find no potential counterpart. Where there is no 'coronal' candidate we have taken the classification of the brightest candidate in the error circle.

5.5 Comparison with previous surveys

The results of this classification method are: 64 (69 per cent) coronal sources, 14 (15 per cent) 'extragalactic' sources, 10 (11 per cent) 'No Man's Land', 4 (4 per cent) 'other' sources and 1 (1 per cent) were 'Unidentified'. These fractions are unchanged by considering the 90 per cent complete sample with count-rates greater than 0.002 counts s^{-1}. When we consider that some of the extragalactic and many of the 'No Man's Land' sources may turn out to be coronal, this result is consistent with extending an order of magnitude fainter in flux the Motch et al. (1997) finding that 85 per cent of the X-ray sources brighter than 0.03 PSPC counts s^{-1} in the Cygnus region of the galactic plane are due to active coronae. The results of our survey are also consistent with earlier high-flux X-ray surveys in the Galactic Plane. The *ROSAT* 'glance' toward the Perseus Arm (Motch et al. 1991) concluded $\geq$50 per cent of its observed sources were coronal in origin whilst ≥10 per cent were extra-galactic, with 40 per cent remaining unidentified. M-stars accounted for ≈ 20 percent of the identified coronal sources and could account for a significant fraction (∼ 20 per cent) of the unidentified sources. We have estimated M-dwarfs to comprise ∼ 25 per cent of the 47 sources in our survey that have coronal counterparts with 2MASS photometry good enough to estimate spectral types. The EGPS (Hertz & Grindlay 1984, Hertz & Grindlay 1988) provided similar results, though with a higher extra-galactic proportion, probably due to their harder energy band.

A number of the coronae seem to have been detected while emitting above their nominal saturation limits. We have taken only those coronal sources for which we have published spectral classifications (SIMBAD) or have estimated spectral types from well-constrained ($\sigma_{J-H} \leq 0.1$) 2MASS colours, and compared their $\log(f_{\rm X}/f_{\rm R})$values with those expected for saturated ($\log(L_{\rm X}/L_{\rm bol})$=−3) coronal MS stars of the same spectral type. The $\log(f_{\rm X}/f_{\rm R})$values expected from saturated ($\log(L_{\rm X}/L_{\rm bol})$=−3) coronal MS stars are fairly insensitive to spectral type (and $B-R$) at −1.7 to −1.8 up to early M-type stars, when they increase rapidly to −1.3 at M5. We have found that 11 (17 per cent) of the 64 sources we have classified as coronal were emitting at a higher $\log(f_{\rm X}/f_{\rm R})$than predicted for a saturated source, 7 (11 per cent) by at least 0.5 dex (a factor 3). If any 'extra-galactic' and 'No Man's Land' sources are actually coronal, most of these must also be emitting above their nominal saturated limits. This suggests that a significant proportion of our detected sources may be active coronae caught while flaring. This is reasonably consistent with the conclusions of Fleming et al. (1995) that approximately one quarter of solar-type stars and half of dMe stars in the EMSS were detected while flaring. Source 91 was actually seen to flare during the observation. It was undetected in the first half of the exposure time, but rose by a factor of at least 30 in ∼ 15 ks to become the third-brightest source in the survey. Its $\log(f_{\rm X}/f_{\rm R})$value increased from < -1.0, where it would fall into the coronal zone to +0.5, where it climbs well into the extragalactic zone.

6 COMPARISON WITH MODELS OF CORONAL CONTRIBUTIONS TO X-RAY SOURCE POPULATIONS

Numerical models that predict the $\log N - \log S$ of stellar sources found in flux-limited X-ray surveys have been produced, based on galactic structure models and the observed X-ray luminosity functions (XLFs) of various classes and ages of stars. Figure 9 compares our observed number-flux relation for the hard band to those predicted by two such models. Such comparisons between these models and survey results can reveal irregularities in the local stellar formation rate (SFR) and inconsistency with the assumed spatial distribution of the sources, particularly the youngest stellar population which are the most X-ray active, and particularly at low galactic latitudes.

The XCOUNT model (Favata et al. 1992) is based on the Bahcall & Soneira galactic structure model, and adopts different scale heights for three age ranges of star (Micela et al. 1993). *Einstein* IPC XLFs are used for each different age and spectral class of star. The Bahcall & Soneira model is derived from optical star counts which are insensitive to the age distribution of the stellar population, whereas the X-ray source counts are strongly dependent upon the number of young stars. Discrepancies between optical and X-ray counts are expected to be strongest near the galactic plane, where the young stars are most concentrated. Even at high galactic latitudes, an over-abundance of "yellow" X-ray-emitting stars has been found (c.f. Sciortino et al. 1995, Hodgkin and Pye 1994), indicating the existence of a young local population not included in the standard Bahcall & Soneira model. It has thus been shown that X-ray counts can put useful constraints on the star formation rate (Micela et al. 1993).

We initially used the XCOUNT model for a constant SFR to predict the number of stellar sources in our survey region. In the PSPC hard-band, for the total area of 2.5deg^2, we derived predictions for the $\log N - \log S$ curves for main-sequence (F–M) stars, giants and RS CVn's. A large source of uncertainty exists due to the spatial density of RS CVn's being poorly defined. The full range of densities obtained from Favata et al. (1995) (3.14×10^{-5} – 1.22×10^{-4} pc^{-3}) was used for the modelling. Following Micela et al. (1993) we derived a prediction of 22–31 (9–13 per deg^2) stellar sources above 0.002 ct s^{-1}. This is approximately half the 44–54 (69%–85% of the 64 hard sources detected in our survey) sources with count-rate > 0.002 count s^{-1} which are coronal following our classification. The relative contribution of each stellar class to the predicted number of X-ray sources is shown in Table 6.

This shows that a constant stellar birthrate XCOUNT model underpredicts the coronal contribution to the $\log N - \log S$ on the Galactic plane. However, the XCOUNT predictions can be reconciled with our observations by assuming that the stellar birthrate has doubled during the last billion years, without any changes on the scale heights. Under this assumption, leaving unchanged the contribution of active binaries, the XCOUNT model predicts 36–44 (14–18 per deg^{-2}) coronal sources that compare better with the observed number of coronal sources. We note that such a change in the stellar birthrate is not unrealistic since it would increase only by 10% the total number of stars in the Galaxy, for an age of the old stellar population in the range 1–10 × 10^9 year, with a small effect on optical number counts.

In the soft-band XCOUNT predicts 2–3 stellar sources above 0.0025 count s^{-1} for a constant SFR, and 3–4 in the case of a doubling of the SFR in the last billion years. These numbers compare well with the 4–5 likely coronal sources (cf. Table 3 and 4) out of the 11 detected in the soft band above the limiting rate (0.0025 count s^{-1}) corresponding to 90% completness of our survey.

Guillout et al. (1996a) have produced a model based on their Besançon evolution synthesis model which self-consistently computes the variation of scale height with age, assuming a constant SFR. As in XCOUNT, a similar three age ranges are defined, within which each spectral class has its own XLF. The more recent *ROSAT* PSPC XLFs are used for most classes. The scale height of the two younger populations is approximately half that applied in XCOUNT, hence the density on the galactic plane is almost doubled. In order to make a comparison with our observation we have

Table 6. The relative contribution of each spectral class to the stellar X-ray source counts predicted by various XCOUNT models. A count-rate threshold of 0.002 PSPC count s^{-1} has been applied.

Sp. Type	Percentage of predicted stellar X-ray sources			
	Constant SFR		Doubled SFR	
	High RS CVn	Low RS CVn	High RS CVn	Low RS CVn
dA				
dF				
dG				
dK				
dM				
Giants				
RS CVn				

used the results in Table 4 of Guillout et al. (1996a) which however are computed in the *ROSAT* broad-band (0.1–2.4 keV). Since for a source of a given X-ray luminosity, the broad-band count-rate is higher than the hard-band count-rate, we have to "re-scale" the Guillout et al. results into the hard-band. The re-scaling is however spectrum-dependent; assuming emission from a single temperature coronal plasma with $\log T = .7$ and $N_{\rm H} = 2 \times 10^{20}$ a hard-rate of 0.0020 count s^{-1} will translate into a broad-rate of 0.0025 count s^{-1}, while for the same temperature and $N_{\rm H} = 4 \times 10^{20}$ a hard-rate of 0.0020 count s^{-1} will translate into a broad-rate of 0.0022 count s^{-1}. Scaling the Guillout et al. results on the basis of the above considerations we predict about 16 and 17.3 coronal sources per $\deg^2$. Predicted coronal source numbers tend to decrease with the softening of the source spectrum, because of the different band-pass.

Thus the Besançon model with a constant SFR produces results that are similar to those obtained with XCOUNT doubling the SFR in the last billion years and both models have similar ability to reproduce the source counts found in our surveys. However the Besançon model prediction does not include a population of RS CVn-like binaries, which could provide a significant contribution to the coronal $\log N - \log S$ in the Galactic Plane (cf. Fig. 9).

While our data allow us to conclude that the density of young stars in the plane is higher than previously thought (e.g. Basu & Rana 1992), they alone cannot constrain the scale height of the young stellar population. The increase of young star density is supported by recent discoveries of nearby young stellar associations through Hipparcos proper motion measurements (e.g. Tucanae Association, ∼10 Myr, at 50pc; Zuckerman & Webb 2000) and through identification of X-ray sources (e.g. Horologium Association, ∼30 Myr, at 60pc; Torres et al. 2000), which suggest there has been an increase in the SFR in the solar neighbourhood in the last 10–100 Myr. The Gould Belt structure also suggests a recent, local 'large scale' episode of star formation (Guillout et al. 1998). Based on our results we can rule out the cases in which the young stellar population is characterized either by large scale-height *and* constant SFR (underpredicting the number of coronal sources) or small scale-height *and* higher local mean SFR in the last billion years (overpredicting the number of coronal sources). The first case being the "standard" XCOUNT discussed above, the second one being the Besançon model with an increasing SFR (Guillout et al. 1996b). Hernandez, Valls-Gabaud and Gilmore (2000) have used Hipparcos data to show that the local SFR may be episodic, rather than following a continuous trend.

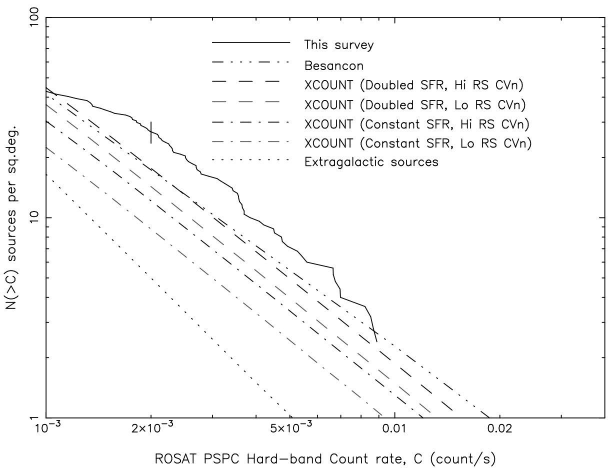

Figure 9. Measured and predicted Galactic Plane $\log N - \log S$ relations. From top to bottom, the curves are: (a) our measured, coverage-corrected $\log N - \log S$; (b) prediction of the Besançon model (Guillout et al. 1996a) corrected for hard band; (c)–(f) predictions of the XCOUNT model, with two different assumptions for the star formation rate in the last 10^9 years and two different assumptions for the density of RS CVn binaries (see §6); (g) estimated contribution from extragalactic sources using a Galactic transmission factor of 0.3 and the high-latitude measurements of Hasinger et al. (1993).

7 SUMMARY

We have performed a soft X-ray survey of the Galactic Plane that is more than an order of magnitude deeper than previous X-ray surveys near the Galactic Plane. A sky area of 2.5 $\deg^2$ was surveyed, yielding 93 sources, 64 with hard-band (0.4–2.0 keV) fluxes $> 2 \times 10^{-14}$ erg cm^{-2} s^{-1} . On the basis of $\log(f_{\rm X}/f_{\rm opt})$ vs optical colour diagrams (USNO-A2.0 and Tycho2) and NIR photometry (2MASS), we found 69 per cent of the sources to have counterparts consistent with being coronal sources, with 15 per cent consistent with extragalactic sources, 10 per cent inconsistent with either of these two classes, 4 per cent to be early-type stars or HII regions and 1 per cent to have no nearby optical or NIR counterpart ($R \lesssim 19$, $J \lesssim 16$).

These results are in agreement with earlier high-flux X-ray surveys in the plane, such as the EGPS and the RGPS, that the majority of sources are consistent with late-type stars, and indicate that active coronae remain the dominant population of X-ray sources more than an order of magnitude fainter in flux than the sensitivity limits of previous studies.

A significant percentage (10–20 per cent) of 'coronal' sources were detected while emitting above their nominal saturated limit ($\log(L_X/L_{bol}) = -3$), consistent with Fleming et al. 's (1995) conclusion that 25 per cent of solar-like stars and 50 per cent of dMe stars were detected while flaring.

Our data allow us to rule out models of stellar X-ray counts in which the young stellar population is characterized either by large scale-height *and* constant SFR or small scale-height *and* increased SFR in the last billion year. The observed count can be equivalently explained with the XCOUNT model by assuming a SFR doubled in the last billion year and including the contribution of active binaries, or with the Besançon model with a constant SFR but without including the contribution of active binaries which, on the other hand, could provide a significant contribution to the coronal number count in the Galactic Plane.

Our results support the view that the population of young stars in the plane is denser than previously thought, and highlight the ability of flux-limited X-ray surveys to map the young stellar component of the Galaxy.

ACKNOWLEDGMENTS

JEM, JPP and KRB acknowledge the financial support of the UK Particle Physics and Astronomy Research Council (PPARC). This work made use of archival material from the SIMBAD and VIZIER systems at CDS, Strasbourg, and the Leicester Database and Archive Service (LEDAS). SS and GM acknowledge support from the Italian Space Agency (ASI) and Ministero della Ricerca Scientifica e Tecnologica (MURST).

REFERENCES

Allan D. J., 1992, ASTERIX User note 004, Starlink, Rutherford Appleton Laboratory
Allen C. W., 1973, *Astrophysical quantities*, London: University of London, Athlone Press, 1973, 3rd ed.
Ayres T. R., Linsky J. L., Vaiana G. S., Golub L., Rosner R., 1981, ApJ, 157, 1157
Basu S., Rana N. C., 1992, ApJ, 393, 373
Belloni T., Mereghetti S., 1994, A&A, 286, 935
Bessell M. S., Brett J. M., 1988, PASP, 100, 1134
Boyle B. J., McMahon R. G., Wilkes B. J., Elvis M., 1995, MNRAS, 276, 315
Branduardi-Raymont G, et al. , 1994, MNRAS, 270, 947
Briggs K. R., Pye J. P., Jeffries R. D., Totten E. J., 2000, MNRAS, 319, 826
Bronfman L., Nyman L., May J., 1996, A&AS, 115, 81
Cash W., 1979, ApJ, 228, 939
Cohen M., Jones B. F., Walker H. J., 1989, ApJ, 341, 908
Cutri R. M., 2000, go to http://www.ipac.caltech.edu/2mass/
Dame T. M., et al. , 1987, ApJ, 322, 706
ESA, 1997, The Hipparcos and Tycho Catalogues, ESA SP-1200, Vol. 1-17
Favata F., Micela G., Sciortino S., Vaiana G. S., 1992, A&A, 256, 86
Favata F., Micela G., Sciortino S., 1995, A&A, 298, 482
Fleming T. A., Molendi S., Maccacaro T., Wolter A., 1995, ApJS, 99, 701
Frisch P. C., York D. G., 1983, ApJL, 271, 59
Gioia I. M., Maccacaro T., Schild R. E., Wolter A., Stocke J. T., Morris S. L., Henry J. P., 1990, ApJS, 72, 567
Guillout P., Haywood M., Motch C., Robin A. C., 1996a, A&A, 316, 89
Guillout P., Haywood M., Motch C., Robin A. C., 1996b, Proc. 'Röntgenstrahlung from the Universe', eds. Zimmermann, H.U.; Trümper, J.; and Yorke, H.; MPE Report 263, 41
Guillout P., Sterzik M. F., Schmitt J. H. M. M., Motch C., Neuhäuser R., 1998, å, 337, 113
Haberl F., Pietsch W., 1999, A&AS, 139, 277
Haberl F., Filipović M. D., Pietsch W., Kahabka P., 2000, A&AS, 142, 41
Haisch B. M., Simon T., 1982, ApJ, 183, 252
Hasinger G., Burg R., Giacconi R., Hartner G., Schmidt M., Trümper J., Zamorani G., 1993, A&A, 275, 1
Hernandez X., Valls-Gabaud D., Gilmore G., 2000, MNRAS, 316, 605
Hertz P., Grindlay J. E., 1984, ApJ, 278, 137
Hertz P., Grindlay J. E., 1988, AJ, 96, 233
Hodgkin S. T., Pye J. P., 1994, MNRAS, 267, 840
Høg E., et al. , 2000, A&A, 355, L27
Johnson H. L., Ann. Rev. Astron. & Astrophys. 1966, 4, 193
Lampton M., Margon B., Bowyer S., 1976, ApJ, 208, 177
Machalski J., Wiśniewski W. Z., 1988, MNRAS, 231, 1065
Micela G., Sciortino S., Favata F., 1993, ApJ, 412, 618
Monet D., et al. , 1998, The PMM USNO-A2.0 Catalog
Morley J., 1998, Ph.D. thesis
Motch C., et al. , 1991, A&A, 246, 24
Motch C., Guillout P., Haberl F., Pietsch W., Reinsch K., 1997, A&A, 318, 111
Motch C., Guillout P., Haberl F., Krautter J., Pakull M. W., Pietsch W., Reinsch K., Voges W., Zickgraf F.-J., 1998, A&AS, 132, 341
Palagi F., Cesaroni R., Comoretto G., Felli M., Natale V., 1993, A&AS, 101, 153
Paresce F., 1984, AJ, 89, 1022
Pfeffermann E., et al. , 1986, Proc. SPIE, 733, 519
Schmidt-Kaler Th., 1982, 'Physical parameters of the stars,' Landolt-Börnstein Numerical data and functional relationships in science and technology, New Series, Group IV, Volume 2b, Springer-Verlag, Berlin
Seeberger R., Saurer W., Weinberger R., 1996, A&AS, 117, 1
Sciortino S., Favata F., Micela G., 1995, A&A, 296, 370
Stark A. A., Gammie C. F., Wilson R. W., Bally J., Linke R. A., Heiles C., Hurwitz M., 1992, ApJS, 79, 77
Stocke J.T., Morris S. L., Gioia I. M., Maccacaro T., Schild R., Wolter A., Fleming T. A., Henry J. P., 1991, ApJS, 76, 813
Torres C. A. O., da Silva L., Quast G. R., de la Reza R., Jilinski E., 2000, AJ, 120, 1410
Trümper J., et al. , 1991, Nature, 349, 579
Zuckerman B., Webb R. A., 2000, ApJ, 535, 959